Conformational Dynamics of the F$_1$-ATPase β-Subunit: A Molecular Dynamics Study

Rainer A. Böckmann and Helmut Grubmüller

Theoretical Molecular Biophysics Group, Max-Planck Institute for Biophysical Chemistry, Göttingen, Germany

ABSTRACT   According to the different nucleotide occupancies of the F$_1$-ATPase β-subunits and due to the asymmetry imposed through the central γ-subunit, the β-subunit adopts different conformations in the crystal structures. Recently, a spontaneous and nucleotide-independent closure of the open β-subunit upon rotation of the γ-subunit has been proposed. To address the question whether this closure is dictated by interactions to neighbored subunits or whether the open β-subunit behaves like a prestressed "spring," we report multinanosecond molecular dynamics simulations of the *isolated* β-subunit with different start conformations and different nucleotide occupancies. We have observed a fast, spontaneous closure motion of the open β_E-subunit, consistent with the available x-ray structures. The motions and kinetics are similar to those observed in simulations of the full $(\alpha\beta)_3\gamma$-complex, which support the view of a prestressed "spring," i.e., that forces internal to the β_E-subunit dominate possible interactions from adjacent α-subunits. Additionally, nucleotide removal is found to trigger conformational transitions of the closed β_{TP}-subunit; this provides evidence that the recently resolved half-closed β-subunit conformation is an intermediate state before product release. The observed motions provide a plausible explanation why ADP and P$_i$ are required for the release of bound ATP and why γ-depleted $(\alpha\beta)_3$ has a drastically reduced hydrolysis rate.

INTRODUCTION

The mitochondrial enzyme F$_o$F$_1$-ATP synthase synthesizes adenosine triphosphate (ATP), the universal currency of chemical energy in the cell. Using the pH-gradient between the cytosolic site and the matrix, the membrane embedded F$_o$-part (ab$_2$c$_{10-14}$, *Escherichia coli* nomenclature) drives the synthesis of ATP in the F$_1$-headpiece ($\alpha_3\beta_3\gamma\delta\varepsilon$, see also Fig. 1 *A*). The latter contains the three nucleotide binding pockets of the enzyme, which are formed mainly by the residues of the three β-subunits. For the reverse (hydrolysis) direction, a rotation of the F$_o$ c-ring consisting of 10–14 identical subunits (Stock et al., 1999; Stahlberg et al., 2001; Seelert et al., 2000) has been observed in the F$_o$F$_1$-ATPase (Sambongi et al., 1999; Pänke et al., 2000). For the isolated F$_1$-part, it has been shown that the hydrolysis of ATP is coupled to a rotation of the central, coiled-coil γ-subunit in 120° steps (Duncan et al., 1995; Sabbert et al., 1996; Noji et al., 1997). These experiments supported the picture of the F$_o$F$_1$-ATP synthase as two tightly coupled, fully reversible rotary motors (Engelbrecht and Junge, 1997; Junge et al., 1997). In synthesis direction, a proton flux across the membrane drives the rotation of the F$_o$ c-ring. This rotary motion is transduced to the F$_1$-motor by the γ- and ε-subunits located between F$_o$ and F$_1$. The peripheral subunits δ and *b*, as parts of the stator, hold the $(\alpha\beta)_3$ hexamer of F$_1$ in a fixed position. Thus, for the synthesis cycle, chemical energy is converted into rotational motion by the F$_o$-part, transmitted by the γ-subunit to the F$_1$-head, and finally reconverted into chemical energy via synthesis of ATP within the three catalytic active sites of the F$_1$-head.

To achieve the almost 100% efficiency of the F$_1$-motor (Yasuda et al., 1998), a tight coupling of the γ-rotation to structural rearrangements in at least one of the three nucleotide binding pockets has been suggested (Oster and Wang, 2000). This picture is supported by the available F$_1$-unit crystal structures (Abrahams et al., 1994, 1996; van Raaij et al., 1996, Orriss et al., 1998; Gibbons et al., 2000; Braig et al., 2000; Menz et al., 2001), which show the three β-subunits in three different conformations. These differ in their particular position with respect to the asymmetrical γ-subunit and their nucleotide occupancy. As shown in Fig. 1 *A*, the binding pocket in one of the three β-subunits (β_E) is empty, the second one (β_{DP}-subunit) contains ADP, and the third one (β_{TP}-subunit) contains the ATP analog AMP-PNP. In the structure by Abrahams et al. (1994), both the β_{TP}- and β_{DP}-subunits are in a closed conformation (*C*) and the empty β_E-subunit is open (*O*). As seen in Fig. 1 *C*, the open conformation shows a large outwards tilt of the lower C-terminal domain by ~26° with respect to the closed conformation. Recently, the F$_1$-ATPase with a half-closed (*HC*) β_{ADP+Pi}-subunit could be resolved which was interpreted as an intermediate state shortly before product release (Menz et al., 2001).

These findings supported models for the binding change mechanism (Boyer, 1981; Cross, 1981; Duncan et al., 1995; Wang and Oster, 1998; Allison, 1998; Menz et al., 2001), for which each of the β-subunits — or binding pockets — is expected to go through (at least) three states during hydrolysis or synthesis. These states differ in their nucleotide affinities: a *tight* state with high ATP affinity, a *loose* state with medium affinity, and an *open* or low affinity state. Assuming that the
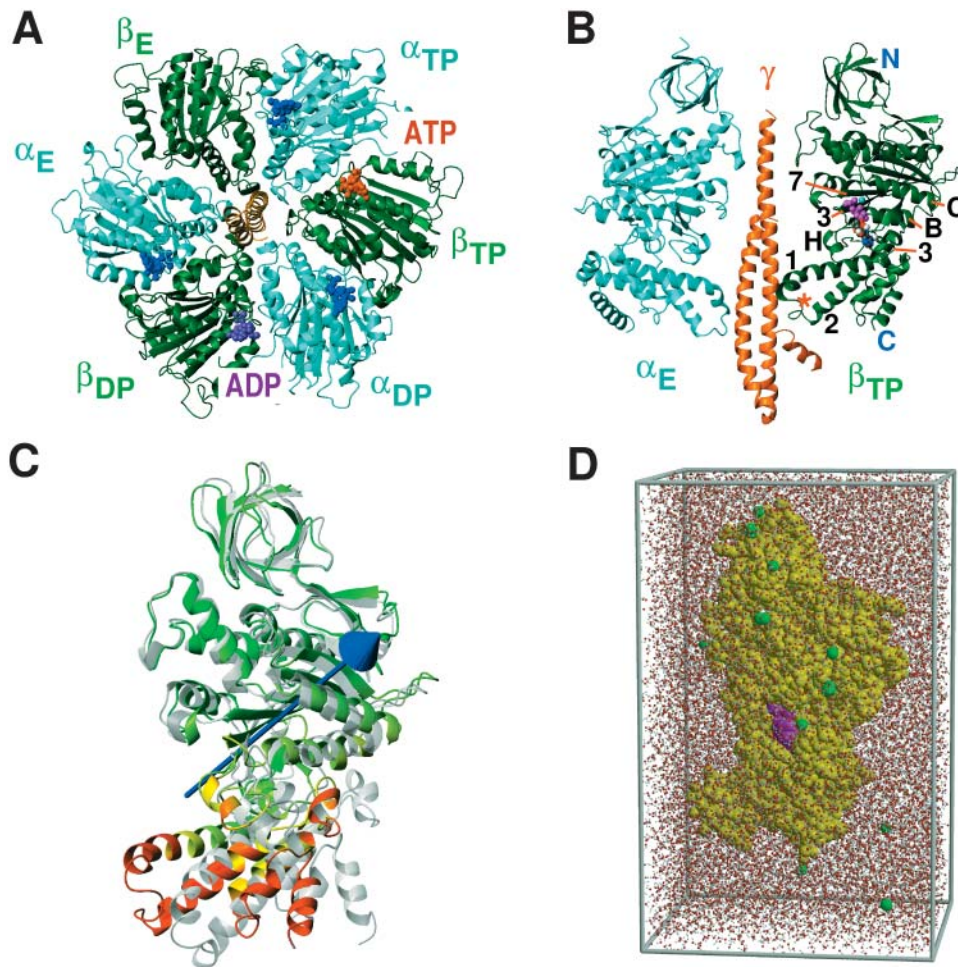

FIGURE 1 $(\alpha\beta)_3\gamma$-complex of the F$_1$-ATPase (Abrahams et al., 1994), as seen from the membrane (*A*) and lateral view of the $\alpha_E\beta_{TP}\gamma$-fragment (*B*) together with notation of specific α-helices (3, B, C, and H) and β-sheets (3 and 7) according to Abrahams et al. (1994). The red star indicates the position of the DELSEED sequence (residues 394–400). Shown in *C* is an overlay of β_{TP}- (*colored*) and β_E-subunit (*gray*), taken from the x-ray structure (Gibbons et al., 2000), after fitting to the N-terminal and the substrate binding domain with the rotation vector representing the domain motion between lower and upper domain as determined by DynDom (Hayward and Berendsen, 1998; Hayward and Lee, 2002). The periodic simulation system for the isolated β-subunit (*yellow*; substrate, *magenta*) in a water box with sodium ions (*green*) is shown in *D*.

$(\alpha\beta)_3\gamma$ x-ray conformation with its specific bound nucleotides resembles a snapshot during the hydrolysis cycle, one can assign the open state to the empty β_E-subunit and the loose and tight states to the two β-subunits in closed conformations (Abrahams et al., 1994). Motivated by this assignment, the large conformational difference between the open and closed β-subunits was generally assumed to be coupled to the different nucleotide occupancies: the substrate-free β-subunit adopts an open conformation, whereas the β-subunit with bound substrate adopts a closed conformation. The transition from the open to the closed conformation was assumed to be driven by nucleotide rebinding to the β_E-subunit, which is empty at this stage of the cycle. For the synthesis cycle, the transition from the closed to the open conformation with subsequent nucleotide release was attributed to the rotation of the γ-subunit.

This view received further support from a nucleotide-free (assembled) $(\alpha\beta)_3$ subcomplex structure from *Bacillus* PS3 (Shirakihara et al., 1997), which shows all β-subunits in open conformation. The latter structure seems to rule out the second possibility mentioned above, namely that the different conformations are dictated by the asymmetrical position of

the γ-subunit with respect to the β-subunits, which might hinder the β_E-subunit from closure as was originally proposed by Abrahams et al. (1994). However, all β-subunits in the recently resolved structure of chloroplast F$_1$-ATPase $((\alpha\beta)_3\gamma\varepsilon$, isolated from natural source), which is also nucleotide-free, adopt a closed conformation (Groth and Pohl, 2001), rendering the above question again undecided.

A recent molecular dynamics simulation study (Böckmann and Grubmüller, 2002; Böckmann, 2002) of the $(\alpha\beta)_3\gamma$-complex of F$_1$ in explicit solvent environment during which the system was driven in synthesis direction, confirmed that the opening of the β_{TP}-subunit with bound ATP is driven by rotation of the γ-subunit by 120°. Interestingly, the closure of the formerly open empty β_E-subunit was found to occur *spontaneously* and fast, without the need for rebinding of phosphate or ADP. These results suggest that the position of the γ-subunit within the $(\alpha\beta)_3$-complex forces the empty β_E-subunit into the open conformation.

The fact that β_E with bound ADP can also close spontaneously might be concluded from a second molecular dynamics study of the F$_1$-ATPase (Ma et al., 2002).

However, this considerably shorter simulation was performed in vacuo with a dielectric coefficient of $\varepsilon = 11$ also for the solvent region. Therefore, one cannot rule out that artificial forces onto surface charges of the β-subunit, which are typically directed toward the interior of the protein in a vacuum simulation, contributed the observed conformational closure motion in this case.

The question arises whether the observed spontaneous closure motion (Böckmann and Grubmüller, 2002) of the β_E-subunit was promoted by specific interactions between the β-subunit and the adjacent α-subunits or by interactions to the γ-subunit. Alternatively, this large-scale motion might be due to internal forces of the β-subunit and thus would rather be comparable to the relaxation or backsnapping of a pre-stressed "spring". To answer these questions and to complement the results seen for the full $(\alpha\beta)_3\gamma$-complex, we performed multinanosecond molecular dynamics simulations of the isolated β-subunit in both open and closed conformations with different nucleotide occupancies in explicit solvent environment. Additionally, the specific influence of the bound substrates (ADP and Mg^{2+}) on the β-conformations have been studied and will be discussed in this report.

METHODS

As start structures, an open and a closed β-subunit (residues 9–474 of β_E and β_{TP}, respectively) were taken from the recently resolved F_1-ATPase at 2.4 Å resolution (Gibbons et al., 2000) (PDB-entry *1E79*). Four different simulation systems were set up (see Table 1); namely the (closed) β_{TP}-subunit with bound ADP and Mg^{2+} (simulation AS), the β_{TP}-subunit with Mg^{2+} (BS), the β_{TP}-subunit with removed substrates (CS), and the (open) β_E-subunit without bound substrate (DS).

All simulations were performed in a periodic box (11.7 nm × 6.5 nm × 7.1 nm); the β-subunits were each solvated with 15,673–15,722 SPC (Berendsen et al., 1981) water molecules (Fig. 1 *D*). Polar and aromatic hydrogen atoms were added to the protein and all other hydrogen atoms were treated via compound atoms. To each of the simulation systems, 16–18 Na^+ ions were added to compensate for the net negative charge of the β-subunit and the substrates.

All MD simulations were carried out using the GROMACS simulation suite (Lindahl et al., 2001). Application of the LINCS (Hess et al., 1997) and SETTLE (Miyamoto and Kollman, 1992) methods allowed for an integration step size of 2 fs. Electrostatic interactions were calculated with the Particle-Mesh Ewald method (PME) (Darden et al., 1993). The system was coupled to an external temperature bath (Berendsen et al., 1984) of 300 K with a coupling constant of $\tau_T = 0.1$ ps separately for the protein, the solvent, and added ions. The pressure was kept constant by a weak coupling to a pressure bath (Berendsen et al., 1984) with $\tau_p = 1$ ps. The GROMACS force field was applied. Each simulation started with an energy minimization using a steepest descent algorithm (20 steps) and was followed by simulations of 100 ps length with harmonic position restraints applied on all protein atoms (force constant 1000 kJ/mol^{-1}nm^{-2}) to allow relaxation of the solvent molecules.

The conformational motions of the four systems were studied by subsequent free dynamics simulations of 12.5 ns length each. Figs. 1 and 4 were prepared with MOLMOL (Koradi et al., 1996), Figs. 6 and 7 with BobScript (Esnouf, 1997), and Raster3D (Merritt and Bacon, 1997).

The correlation coefficient ν for the B-factor $B^{S,X}$ of a group of N residues between simulation (index S) and x-ray structure (index X) was calculated as

$$\nu = \frac{\sum_{i=1}^{N}[(B_i^S - \bar{B}^S)(B_i^X - \bar{B}^X)]}{\sqrt{\sum_{i=1}^{N}(B_i^S - \bar{B}^S)^2} \times \sqrt{\sum_{i=1}^{N}(B_i^X - \bar{B}^X)^2}}. \qquad (1)$$

As a measure for the overlap of the conformational subspaces sampled by the simulations and by the x-ray structures of the β-subunit, the normalized overlap σ of the respective covariance matrices M was used,

$$\sigma = 1 - \frac{\sqrt{\text{tr}(\sqrt{M_K} - \sqrt{M_S})^2}}{\sqrt{\text{tr}(M_K) + \text{tr}(M_S)}}, \qquad (2)$$

where the indices K and S distinguish between the covariance matrices for the crystal structure (K) and the simulation (S), respectively. This overlap measure is 1 for identical matrices and 0 for orthogonal matrices.

RESULTS AND DISCUSSION

During the free dynamics simulations, the root mean-square deviations (RMSD) of the backbone atoms from the respective initial structures were monitored. During the first 100 ps, each system shows a steep increase in the RMSD (see Fig. 2 and Table 2) to a typical value of 1.5–2 Å. As can be seen, the system that starts from the closed β_{TP}-conformation with bound ADP and Mg^{2+} (system AS) then remains relatively close to the starting structure at an RMSD value of ~2.3 Å. Hence, the β_{TP}-conformation is not only stable in the $(\alpha\beta)_3\gamma$-complex, but also as an isolated β-subunit with bound substrate. This can also be seen from the intactness of the secondary structure (data not shown). In contrast, the β-subunit in the simulation of the closed β-subunit without substrate (system CS), and of the empty open β_E-subunit, undergo significant conformational transitions (*gray* and *black dashed lines* in Fig. 2), as can be seen from the relatively large RMSD values of 3.3 Å and 4.4 Å, respectively. As will be analyzed in more detail below, this increase is caused by a large motion mainly of the C-terminal domain (residues 364–474), which, however, also leaves the secondary structure nearly unchanged (data not shown).

The atomic fluctuations of the C-terminal region calculated from the final 10 ns of each trajectory (see Methods) correlate convincingly with the crystallographic B-factors
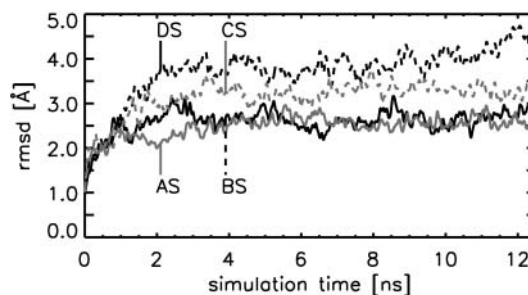

FIGURE 2   Root mean-square deviation (RMSD) of the backbone atoms from the respective starting structures during the simulations (compare to Tables 1 and 2). Solid lines refer to systems AS (*gray*) and BS (*black*), respectively; dotted lines refer to (empty) systems, CS (*gray*) and DS (*black*).

TABLE 1 Simulated systems

System	AS	BS	CS	DS
Subunit and substrate	β_{TP}-ADP + Mg^{2+}	β_{TP}-Mg^{2+}	β_{TP}	β_E
Start conformation	C	C	C	O
Total number of atoms	51,438	51,446	51,441	51,588
thereof				
protein	4,404	4,404	4,404	4,404
ADP	32	0	0	0
Mg^{2+}	1	1	0	0
water	46,983	47,025	47,019	47,166
NA$^+$ ions	18	16	18	18

Composition of simulated systems of the isolated β-subunits of the F$_1$-ATPase.

(correlation coefficients 0.63–0.71, see Table 3). For the nucleotide binding domain (residues 82–363), much weaker correlations of 0.11–0.31 are seen. Such weak correlation would indeed be expected from the arrangement of the β-subunits within the F$_1$-complex: at the position of the nucleotide binding domain, the β-subunits have maximal contact to the adjacent α-subunits, which are not included within the simulation systems. Interestingly, the best agreement is obtained for the DELSEED region (residues 394–400) and the adjacent helices 1 and 2. Here, the correlation coefficient for the simulations of the β_{TP}-subunit is 0.66–0.71 and even 0.82 for the β_E-subunit (Fig. 3). In this C-terminal region, the influence of the neighbored α-subunits is smaller and allows for enlarged mobilities in the crystal structure, comparable to the situation in the simulation. For the crystal β_E-subunit, this effect is even enhanced due to the outwards tilt of this region (see Fig. 1 C), which further reduces the influence of the α-subunits. Therefore, the presence or absence of adjacent α-subunits has only little effect on the dynamics of the C-terminal part of the β-subunit.

The superposition of the respective final simulation structures (averaged over 100 ps) with the corresponding x-ray structures (Fig. 4) shows only small changes for the simulation of the closed β_{TP}-subunit with bound ADP and

Mg^{2+} (AS), suggesting that the adjacent α-subunits and the γ-subunit are not essential for the conformational stability of the β-subunit.

For the ADP-depleted closed β_{TP}-subunit (simulations BS and CS), we observe large conformational changes of the lower C-terminal domain (colored *red* in Fig. 4). These changes are quite similar to each other. The RMSDs of the final simulation structures to the x-ray C-conformation (*gray*) are 2.8 and 3.3 Å (see Table 2), respectively, i.e., much larger than the deviation of only 1.8 Å between the two final structures.

As can also be seen in Fig. 4 (BS, CS), substrate removal changes especially the orientation of helices 1 and 2 (connected by the DELSEED sequence) with respect to the N-terminal and nucleotide binding domain, such that the C-terminal region bends toward the open conformation by up to 4.4 Å (DELSEED region, after fitting to the N-terminal and nucleotide binding domain). This opening motion is combined with a counterclockwise pivoting of that region (viewed from the membrane side) toward the α_{TP}-subunit as visible in the bottom row of Fig. 4.

The motions of that region in the open β_E-subunit (simulation DS) are quite similar, but proceed in reverse direction. Here, the C-terminal region moves the large distance of more than 15 Å toward the closed conformation (*top row*) and pivots sidewards toward the adjacent α_{TP}-subunit (*bottom row*). A similar rotation is observed for the short helix H close to the binding pocket.

The angle between helices B and C increases during the simulations BS, CS, and DS. For the simulations of the closed β-subunit with removed substrates (BS and CS), helix B tilts with respect to helix C, in case of the β_E-subunit (DS) helix C with respect to helix B. Helix 3 — adjacent to the nucleotide binding domain — exhibits a large flexibility especially for the simulation of the empty β_{TP}-subunit and the open β-subunit. The orientation of the central β-barrel domain remains close to its initial conformation in all simulations.

TABLE 2 RMS deviations from x-ray structures

		RMSD [Å] Fitted to conformation		
Simulation	Subunit	O	C	H-C
AS	β_{TP}	4.4	2.3	3.5
BS	β_{TP}	3.9	2.8	2.8
CS	β_{TP}	4.4	3.3	3.2
DS	β_E	4.4	3.6	4.4
	β_{TP}	3.6	0.0	2.9
	β_E	0.0	3.6	1.8

Root mean square deviations (using backbone atom positions of residues 9–126 and 129–464) of averaged final simulation structures from the three β-x-ray conformations, i.e., open (O), closed (C), and half-closed (H-C). The last two lines give the deviations of the respective x-ray β-conformations from each other.

TABLE 3 B-factor correlation coefficients to x-ray structure

	Simulation system			
Domain	AS	BS	CS	DS
N-terminal domain	0.41	0.60	0.37	0.52
β9–81	(0.18)	(0.41)	(0.20)	(0.35)
Nucleotide domain	0.11	0.18	0.25	0.13
β82–363	(0.28)	(0.22)	(0.31)	(0.22)
C-terminal domain	0.67	0.63	0.73	0.71
β364–474	(0.64)	(0.61)	(0.70)	(0.68)
Total system	0.31	0.34	0.49	0.49
β9–474	(0.38)	(0.39)	(0.50)	(0.49)

Correlation coefficients between (residue-averaged) B-factors from the crystal structure and calculated B-factors from the last 10 ns of the corresponding free dynamics simulations. Shown are the correlation coefficients to the open β_E-subunit and (in parentheses) to the closed β_{TP}-subunit.
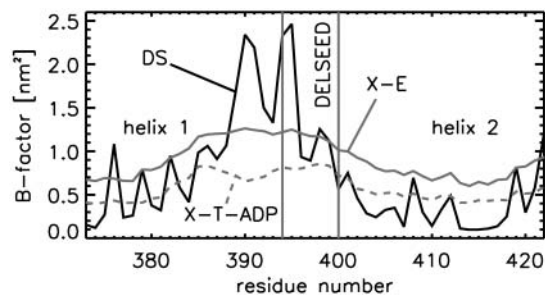
FIGURE 3   Comparison of the B-factors (averaged over atoms of the residues) from the β_E (*X-E, gray*) and β_{TP} (*X-T-ADP, dashed gray line*) x-ray structures with the B-factors computed from the MD trajectory of the initially open β_E-subunit (*DS, black solid line*). The residue range of the DELSEED sequence is marked through vertical lines. The regular pattern on both sides of the DELSEED region is caused by the predominantly α-helical conformation of these residues.

The conformational changes described above provide further evidence for a fast and spontaneous, nucleotide-independent closure of the open β_E-subunit (Böckmann and Grubmüller, 2002) and suggest that, despite the comparatively slow observed turnover rate (Yasuda et al., 2001), the actual conformational transitions, e.g., triggered by substrate removal in the closed β_{TP}-subunit, can proceed at an ns timescale. It is worth re-emphasizing that the latter changes are not just localized within the nucleotide binding region,

but propagate further up in the C-terminal domain by 3 nm as visible in the bottom row of Fig. 4. The timing of these motions will be analyzed in more detail further below.

To distinguish between fluctuations of small amplitudes and domain motions of large amplitudes, we determined the essential conformational subspaces (Amadei et al., 1993) sampled in the simulations by diagonalization of the mass-weighted co-variance matrix (using the heavy backbone atoms) for the four simulations. As can be seen in Fig. 5, the largest eigenvalue for the open subunit (simulation DS, *black*) is significantly larger than the respective values for the three simulations of the closed β-subunit (*gray lines*). As shown in the cumulative representation (*inset*), the motion along the corresponding eigenvector accounts for ~41% of the total motion, which is also larger than for the closed subunit (26% for AS, 19% for BS, and 30% for CS).

The domain motions obtained from the simulations were identified and quantified with the program DynDom (Hayward and Berendsen, 1998; Hayward and Lee, 2002), which allows us to determine protein domains involved in hinge bending motions (Fig. 6). Shown are the domains (*red* or *blue*) that are identified as moving relative to each other, the bending residues (residues at the interdomain boundary, colored *yellow*), and the respective rotation vectors; the color of the arrowhead denotes the particular moving domain (right-hand rule). Comparison of the crystal β_E-subunit with the (averaged) final structure of the open β_E-subunit obtained
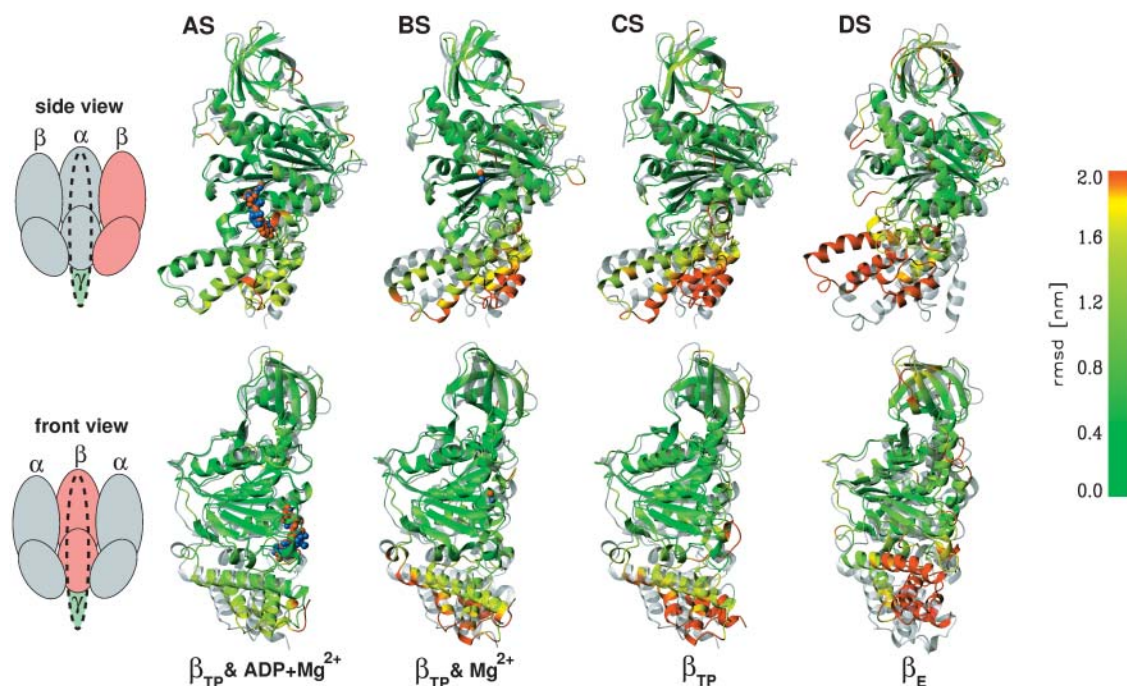

FIGURE 4   Conformational changes seen in the simulations AS, BS, CS, and DS. Shown are the used crystal structures (*gray*) and the final simulation structures (*colored*, averaged over 100 ps). The color-code shows RMS deviations (large deviations, *red*; small deviations, *green*) from the crystal structures after fitting to the N-terminal and nucleotide binding domain (residues 9–363). Substrates of the crystal structure are colored blue, those from the simulations orange. The upper row shows the β-subunits viewed from the adjacent α-subunit, the lower row as viewed from the central γ-subunit.
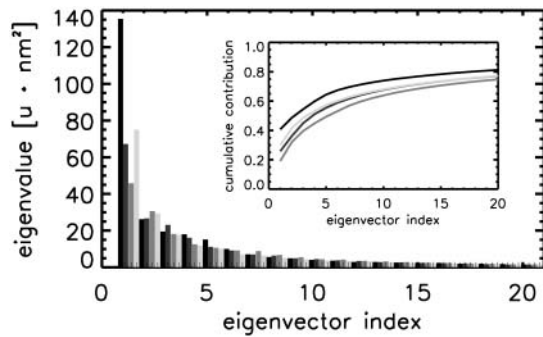
FIGURE 5 Comparison of the fluctuations of the β-subunit. Shown are the eigenvalues of the mass-weighted co-variance analysis for each simulation (DS, *black*; AS, BS, and CS, *dark* to *light gray*) as well as their cumulative contribution to the total conformational change (*inset*).

from simulation DS reveals a 22.2° rotation of the lower C-terminal domain and parts of the nucleotide binding domain with respect to the head region (Fig. 6 *A* and Table 4). The rotation vector — referred to as θ-axis in the following — can be decomposed in a component parallel and in a component perpendicular to the γ-subunit in the F$_1$-complex. The former describes a (clockwise) pivoting motion of the C-terminal domain toward the adjacent α_{TP}-subunit in the F$_1$-complex, the latter a large upwards-tilting of the C-terminal domain, i.e., the closure motion. The closure motion is similar to the one described by the rotation vector obtained by comparing the open x-ray β-conformation with the closed one (Fig. 6 *D*); the rotation vectors differ by an angle of 26°. As can be seen in Fig. 6 *B*, the first eigenvector of simulation DS describes this large domain motion to nearly full extent; almost the same domains (see Table 4) move with respect to each other and the respective

rotation vectors are almost parallel (angle $\approx$ 5°). Large changes in main-chain dihedral angles (data not shown) were observed for residues 177–179, comparable to those determined from a comparison of open and closed crystal structures. It was previously shown that simultaneous mutation of these hinge residues (position marked by a *black arrow* in Fig. 6 *D*) resulted in almost complete loss of ATPase activity (Masaike et al., 2000).

The rotation vector for the domain motions in simulation CS (β_{TP} without substrate, Fig. 6 *C*) includes an angle of 69° to the one described before for the β_E-subunit. It intersects the central β-sheet at the β_7-strand. As already analyzed above, the rotation around this vector—referred to as ϕ-axis in the following—describes a pivoting by $\sim$18° of the lower C-terminal domain (counterclockwise). Here, the fixed (*blue*) and the moving domain (*red*) meet at the nucleotide binding pocket. The assignment of these domains (see Table 4) differs from that for the simulation of the β_E-subunit in that helix B — and not helix C, as in simulation DS — tilts simultaneously with the C-terminal domain.

Fig. 7 (*right panel*) shows how the motions of the C-terminal domain proceed as a function of time, as described by the two angles that are defined by the two axes θ and ϕ (Fig. 7, *left*), and compares it to those obtained from the respective x-ray structures. As can be seen, the ADP/Mg^{2+}-loaded β_{TP}-subunit (AS) remains close to the initial conformation, whereas the open β_E-subunit reaches the closed conformation ($\theta = 17.8$°) within 2 ns (DS). Interestingly, the substrate-free β_{TP}-subunit (CS) approaches the recently resolved half-closed β_{ADP+Pi}-conformation ($\phi = 15.6$°) also within 2 ns. The β_{TP}-subunit with removed ADP (BS) takes an intermediate position with respect to the ϕ-angle, which may be due to a slower conformational transition that cannot be observed on the simulated timescale.
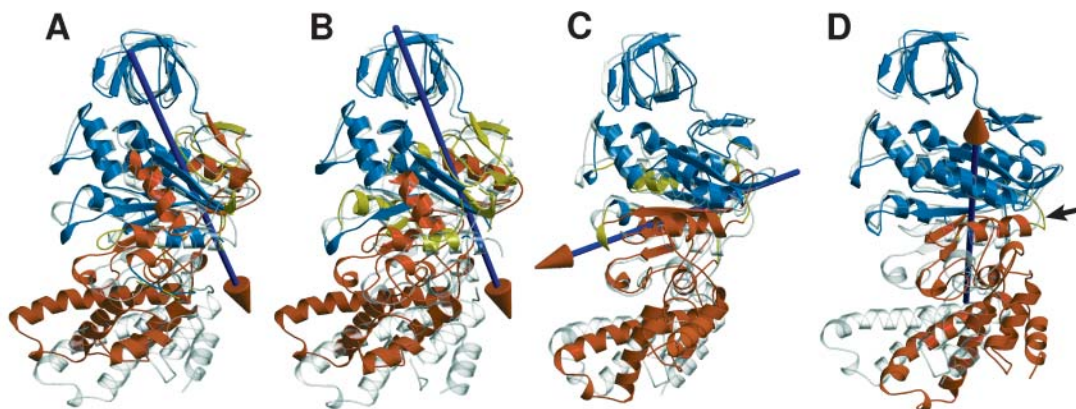

FIGURE 6 Domain movements in the β-subunit from simulation (*A–C*) and crystal structure (*D*). Shown are overlays of initial (*gray*) and final structures (*colored*) of simulation DS (β_E, *A*), of the extreme projections on the first eigenvector of simulation DS (*B*), of the initial and final structures of simulation CS (β_{TP} without substrate, *C*) and of the β_E- (*colored*) and β_{TP} subunits (*D*) from the x-ray structure (Gibbons et al., 2000). The colored arrows indicate the rotation vector for the domain motions necessary to map the initial (*gray*) structures on the final (*colored*) conformations. The blue domains are kept fixed and are used for fitting the respective structures on each other. Bending residues are yellow. The black arrow in *D* points to the hinge region (residues 177–179) for the closure motion (Masaike et al., 2000).

TABLE 4   Domain motion analysis

	Simulation CS	Simulation DS	Simulation DS, 1. eigenvector	β_{TP}/β_E Crystal structure
Fixed domain	17–85, 89–125, 179–242, 251–255, 260–281, 298–303, 319–323	10–83, 96–103, 114–123, 126–128, 147–156, 168–178, 180–191, 211–235, 253–295, 306–330, 356–357, 427–433	11–82, 154–156, 169–171, 175–190, 216–232, 254–296, 307–317	10–132, 173–330
Moving domain	86–88, 132–177, 243–250, 256–257, 295–297, 304–313, 324–473	84–95, 104–113, 124–125, 129–146, 157–167, 178, 192–210, 236–252, 296–305, 331–355, 358–426, 434–473	128–153, 156–168, 172–174, 191–206, 233–253, 297–306, 331–472	133–172, 331–473
Bending residues	85, 86, 88, 89, 125–132, 177–179, 242, 243, 250, 251, 255–260, 281–295, 297, 298, 303, 304, 313–319, 323, 324	83–84, 95–96, 103–110, 113–114, 123–129, 146–147, 156–161, 167–168, 176–180, 191–192, 210–214, 235–236, 252–253, 295–296, 305–306, 330–331, 335–358, 426–430, 433–434	82–128, 153–156, 168–169, 171–172, 174–175, 190–191, 206–216, 232–233, 253–254, 296–297, 306–307, 317–331	132–133, 172–179, 330–331
Angle of rotation	17.9°	22.2°	26.7°	26.2°
%/Closure motion	87.1	54.2	40.2	66.5

Domain analysis of the substrate-free β_{TP} simulation (CS), of the β_E simulation (DS), and comparison with the crystal structure domain analysis between open and closed conformations. In the case of the simulations, start structure and averaged final simulation structure were considered. Additionally, the fourth column gives the respective domain analysis for the extreme projections of the trajectory (simulation DS) on the first eigenvector of the covariance matrix.

The fact that the spontaneous conformational transitions of the isolated β-subunits occur on very similar timescales as those seen for the closure motion observed in the simulation of the $(\alpha\beta)_3\gamma$-complex (Böckmann and Grubmüller, 2002) suggests that the main driving force for the closure is internal to the β-subunit, and not exerted from the adjacent α-subunits.

Note that the observed conformational motions might be affected by artificial interactions with the respective periodic images of the simulation box. To check for such possible artifacts, we have carried out four further simulations with different starting conditions: three of the open β_E-subunit (8, 11, and 14 ns long, using differing initial velocities) and one of the closed β_{TP}-subunit with removed substrate (14 ns
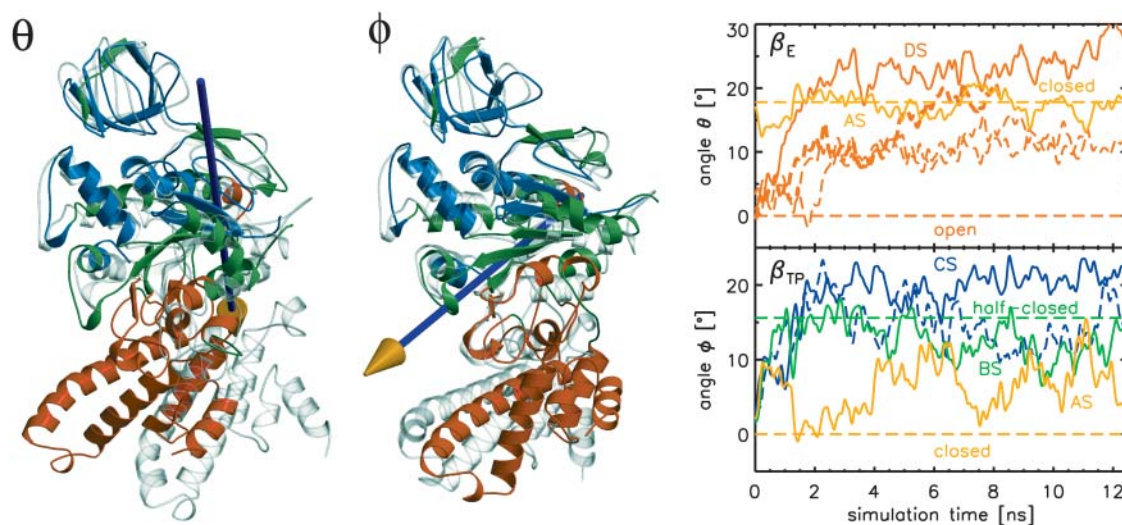

FIGURE 7   Main domain motions in the simulations described by angles θ (*left*) and ϕ (*mid*) between upper (residues 17–83, 96–103 114–123, 180–191, 211–235, 260–281, 319–323, colored *blue*) and lower (residues 132–146, 157–167, 243–250, 331–355, 358–426, 434–473, *red*) domain as a function of simulation time (*right*). The horizontal dashed lines denote the respective angles from the x-ray β-conformations. The angles θ and ϕ were determined independently from each other. The dashed lines show the results from the control simulations in a larger water box (see text).

length). These simulations were carried out with an enlarged water box (>71,000 atoms); the periodic images are ~2.6 ± 0.2 nm apart from each other versus 1.8 ± 0.3 nm for simulations AS–DS. Also the three control simulations of the β_E-subunit display spontaneous closure motions (*dashed lines* in Fig. 7). One of them (*thick dashed line*) reaches a closure angle θ similar to the one seen in simulation DS or in the closed x-ray conformation; the other two remain at a somewhat smaller angle ($\theta \approx 12°$) during the simulation time. For the β_{TP} control simulation, similar pivoting motions are seen as for simulation CS. These results indicate that the closure and pivoting motions are not just accidental, but mostly reproducible at the simulated timescale.

Table 5 quantifies to what extent the conformational transitions seen in the simulations resemble those derived from the x-ray structures (open, closed, and half-closed, respectively) by listing the scalar products (absolute values) of the first eigenvector ($\vec{E}$) of the respective simulation with the difference vectors connecting the particular crystal structures in 3N-dimensional space (N the number of back-bone atoms). Such analysis primarily focuses at the similarity of the main conformational motions (in this case, the closure motion) rather than putting equal weight to all fluctuations, as would be the case for RMSD values. Again, in simulation DS, the open conformation exhibits a large movement in the directions connecting the β x-ray con-formations, as can be seen from the large scalar products of 0.367 and 0.373 between the (normalized) first eigenvector of the β_E-simulation with the one connecting the closed with the open x-ray conformation and the half-closed x-ray conformation, respectively. To judge this number, note that the scalar product between uncorrelated motions follows a Gaussian distribution of 0.015 half-width. Such large overlap (0.289) is also seen for the projection of simulation CS (β_{TP}-subunit with removed substrate) on the vector connecting the closed with the half-closed conformation. Similarly, large values for the normalized overlap σ (see Methods) between the covariance matrices of simulations and crystal structures are seen for simulations CS and DS.

Fig. 8 provides a graphical overview by projecting the four simulation trajectories onto the two-dimensional subspace
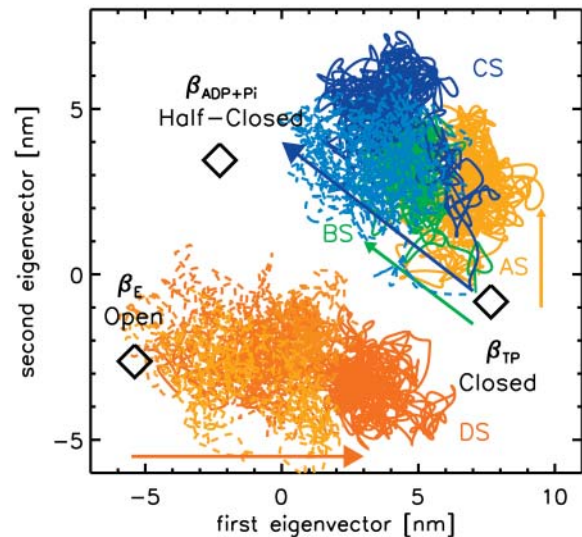

FIGURE 8 Projection of simulation trajectories (*colored lines*) onto the subspace spanned by the x-ray structures of the closed, open, and half-closed β-conformations (*diamonds*). The respective projections of the control simulations are shown as dashed lines; colored light blue for the β_{TP}-subunit without substrate and in light red colors in case of the three β_E control simulations.

defined by the three different x-ray conformations of the β-subunit. As can be seen, the conformation of the open β_E-subunit (simulation DS, *red*) approaches the closed x-ray conformation even up to 80%. Additionally, the confor-mational transitions triggered by removal of the substrate from the closed β_{TP}-subunit approach the half-closed conformation to a significant extent (simulations BS and CS, *green* and *blue curves*, respectively). This result underscores the strong influence of both ADP and Mg^{2+} on the con-formation of the β-subunits.

Although both systems, CS and DS, are identical in that they lack any substrate, they adopt different conformations during the simulations, because they start from different structures (closed/open, respectively). Both adopt a closed-like conformation in that their C-terminal domains are bent upwards toward the N-terminal headgroups but differ in the pivoting ϕ-angle by >30°. We suggest that there exists an energy barrier located between these two states that prohibits completion of the conformational motion within the simulation timescale, and which is overcome upon substrate binding to the empty β_E-subunit or, in the F$_1$-complex, lowered by interactions to the adjacent α-subunits. This view is supported by the observation that the tilt angle between the helices B and C near the binding pocket is increased from 45° to 67° in the simulation of the empty β_E-subunit, rather than decreased as one would expect from comparison to the closed conformation (tilt angle 25°). Remarkably, for the closed β-subunit without substrate (simulation CS), this angle is increased to 34°, exactly the value found for the crystal half-closed conformation (Menz et al., 2001). In this

TABLE 5 Projection of simulation on x-ray structure

Simulation system	$\vec{E}_1 \cdot (\vec{\beta}_{TP} - \vec{\beta}_E)$	$\vec{E}_1 \cdot (\vec{\beta}_{TP} - \vec{\beta}_H)$	σ_{C-O}	σ_{C-H}
AS	0.093	0.005	0.028	0.002
BS	0.044	0.040	0.012	0.012
CS	0.172	0.289	0.056	0.111
DS	0.367	0.373	0.152	0.176

Scalar product (absolute values) of the first eigenvector ($\vec{E}_1$) of simulations AS, BS, CS, and DS, respectively, with the difference vectors connecting the particular crystal structures in 3N-dimensional space (N is the number of backbone atoms). Here, we considered the vectors connecting the closed β-conformation (PDB entry 1E79) with the open ($\vec{\beta}_{TP} - \vec{\beta}_E$)and with the half-closed β-crystal structure ($\vec{\beta}_{TP} - \vec{\beta}_H$). The last two columns show the normalized overlap of the covariance matrix from the simulations with the particular difference vector (σ_{C-O} and σ_{C-H}).

context, it will be interesting to see if the closure motion of the β_E-subunit is indeed completed upon re-insertion of substrate into the binding pocket. However, such study is outside the scope of this report.

SUMMARY AND CONCLUSIONS

Four multinanosecond simulations of the isolated β-subunit of the F_1-ATPase have been carried out, starting from both the open conformation (β_E) and the closed conformation (β_{TP}), with bound ADP and Mg^{2+} (as found in the x-ray structure of the F_1-complex), with Mg^{2+} only, and without substrate.

Unperturbed by any bias or steering, the open β_E-subunit underwent a large spontaneous conformational change toward the closed crystal β-conformation. In particular, the C-terminal domain bent toward the N-terminal domain by >20° within ns. This fast and spontaneous closure motion is similar to the one induced by rotation of the γ-subunit in simulations of the full $(\alpha\beta)_3\gamma$-complex (Böckmann and Grubmüller, 2002). This supports the view that the empty open β_E-subunit adopts a conformation in the F_1-complex that resembles a prestressed "spring," quite in contrast to the common assumption, which attributes the observed differences in the β-conformations rather to the different nucleotide occupancies. The similar kinetics found for both the isolated β_E-subunit and the full complex suggest that the internal tension of the β_E-subunit dominates possible forces originating from interactions with adjacent α-subunits or the γ-stalk.

We note that our use of the notion of a prestressed "spring" does not imply that the underlying potential of mean force is necessarily harmonic — most likely it is not. Rather, this term implies only that the free energy of the closed conformation is lower than that of the open one.

In recent fluorescence experiments it was found that the F_1-ATPase changes its conformation upon phosphate release (Masaike et al., 2002). In our simulations, removal of ADP and Mg^{2+} from the binding pocket of the closed β_{TP}-subunit triggered a spontaneous sidewards pivoting motion of the β_{TP}-subunit, which does not occur with the substrates in place. Also, this motion proceeded spontaneously within ns. Notably, removal of ADP *and* Mg^{2+} from the closed β_{TP}-subunit led to slightly larger conformational changes as compared to those seen upon removal of ADP only. The obtained structure resembles the newly resolved half-closed crystal β_{ADP+Pi} conformation and thus supports the interpretation (Menz et al., 2001) that the β_{ADP+Pi} conformation is an intermediate state shortly before product release.

Our simulations reveal spontaneous or substrate-dependent conformational motions. Both have implications for the transmission of torque (Menz et al., 2001) in the F_1F_o-ATP synthase. Considering the three β-subunits as mechanical devices in the F_oF_1-ATP synthase for the synthesis direction, the spontaneous back-snapping of the lower C-terminal domain of the empty β_E-subunit will likely support the clockwise rotation of the γ-subunit (seen from the membrane). We therefore suggest that the reset, which is required to start the next cycle, consists of the sidewards pivoting motion, described here by a change in the ϕ-angle, and is triggered by binding of new substrate (ADP and P_i) to this subunit. For the *reverse hydrolysis* cycle, this pivoting motion is suggested to be the crucial step during the "power stroke" that drives γ-rotation after binding of ATP to the empty β-subunit. In this direction, the reset is achieved through the spontaneous closure of the β_E-subunit.

These findings also have implications for the binding change mechanism, which deserve further studies. In particular, our model for the synthesis considers both the γ-rotation induced by the F_o-unit and the active support of this rotation by tilting and pivoting of the β-subunits and thereby can explain why ADP and P_i are required for the release of bound ATP (Hackney and Boyer, 1978) and why an electrochemical gradient alone is not sufficient to promote subunit rotation (Zhou et al., 1997). Additionally, in the hydrolysis direction, the mechanical coupling between the γ-enforced opening of a closed β-subunit and vice versa, the β-supported γ-rotation, might explain the drastically reduced hydrolysis rate of γ-depleted $(\alpha\beta)_3$ (Miwa and Yoshida, 1989). The fast spontaneous closure of the substrate-free β_E-subunit — and thus the short lifetime of the open conformation — offers a simple explanation for the observed occupation of all three catalytic sites under maximum turnover conditions in tryptophane fluorescence studies (Weber et al., 1993), although the empty site shows very low affinity. Presumably, the intermediate closed-like conformation of the β_E-subunit seen in the simulations has an enlarged ATP affinity with respect to the open conformation and thus ensures, together with the fast conformational transition, fast rebinding of the substrate.

REFERENCES

Abrahams, J. P., S. K. Buchanan, M. J. van Raaij, I. M. Fearnley, A. G. W. Leslie, and J. E. Walker.1996. The structure of bovine F_1-ATPase complexed with the peptide antibiotic efrapeptin. *Proc. Natl. Acad. Sci. USA.* 93:9420–9424.

Abrahams, J. P., A. G. W. Leslie, R. Lutter, and J. E. Walker. 1994. Structure at 2.8 Å resolution of F_1-ATPase from bovine heart mitochondria. *Nature.* 370:621–628.

Allison, W. S. 1998. F_1-ATPase: A molecular motor that hydrolyzes ATP with sequential opening and closing of catalytic sites coupled to rotation of its γ-subunit. *Acc. Chem. Res.* 31:819–826.

Amadei, A., A. B. M. Linssen, and H. J. C. Berendsen. 1993. Essential dynamics of proteins. *Proteins.* 17:412–425.

Berendsen, H. J. C., J. P. M. Postma, W. F. Van Gunsteren, and J. Hermans. 1981. Interaction Model for Water in Relation to Protein

Hydration. D. Reidel Publishing Company, Dordrecht, The Netherlands. pp.331–342.

Berendsen, H. J. C., J. P. M. Postma, W. F. van Gunsteren, A. D. Nola, and J. R. Haak. 1984. Molecular dynamics with coupling to an external bath. *J. Chem. Phys.* 81:3684–3690.

Böckmann, R. A. 2002. Molekulare Dynamik von Proteinen: Von der α-Helix zur ATP Synthase. Cuvillier Verlag, Göttingen. (PhD thesis.)

Böckmann, R. A., and H. Grubmüller. 2002. Nanoseconds molecular dynamics simulation of primary mechanical energy transfer steps in F$_1$-ATP synthase. *Nat. Struct. Biol.* 9:198–202.

Boyer, P. D. 1981. Energy Coupling in Photosynthesis. Elsevier, Amsterdam, The Netherlands. pp.231–240.

Braig, K., R. Menz, M. Montgomery, A. Leslie, and J. Walker. 2000. Structure of bovine mitochondrial F$_1$-ATPase inhibited by Mg^{2+} ADP and aluminum fluoride. *Struct. Fold. Des.* 8:567–573.

Cross, R. L. 1981. The mechanism and regulation of ATP synthesis by F$_1$-ATPases. *Annu. Rev. Biochem.* 50:681–714.

Darden, T., D. York, and L. Pedersen. 1993. Particle-Mesh Ewald—an $N\log(N)$ method for Ewald sums in large systems. *J. Chem. Phys.* 98:10089–10092.

Duncan, T. M., V. V. Bulygin, Y. Zhou, M. L. Hutcheon, and R. L. Cross. 1995. Rotation of subunits during catalysis by *Escherichia coli* F$_1$-ATPase. *Proc. Natl. Acad. Sci. USA.* 92:10964–10968.

Engelbrecht, S., and W. Junge. 1997. ATP synthase: a tentative structural model. *FEBS Lett.* 414:485–491.

Esnouf, R. M. 1997. An extensively modified version of MOLSCRIPT that includes greatly enhanced coloring capabilities. *J. Mol. Graph. Model.* 15:132–134.

Gibbons, C., M. G. Montgomery, A. G. W. Leslie, and J. E. Walker. 2000. The structure of the central stalk in bovine F$_1$-ATPase at 2.4 Å resolution. *Nat. Struct. Biol.* 7:1055–1061.

Groth, G., and E. Pohl. 2001. The structure of the chloroplast F$_1$-ATPase at 3.2 Å resolution. *J. Biol. Chem.* 276:1345–1352.

Hackney, D. D., and P. D. Boyer. 1978. Subunit interaction during catalysis—implications of concentration dependency of oxygen exchanges accompanying oxidative-phosphorylation for alternating site cooperativity. *J. Biol. Chem.* 253:3164–3170.

Hayward, S., and H. J. C. Berendsen. 1998. Systematic analysis of domain motions in proteins from conformational change: new results on citrate synthase and T4 lysozyme. *Proteins.* 30:144–154.

Hayward, S., and R. A. Lee. 2002. Improvements in the analysis of domain motions in proteins from conformational change: DynDom version 1.50. *J. Mol. Graph.* 21:181–183.

Hess, B., H. Bekker, H. J. C. Berendsen, and J. G. E. M. Fraaije. 1997. LINCS: a linear constraint solver for molecular simulations. *J. Comp. Chem.* 18:1463–1472.

Junge, W., H. Lill, and S. Engelbrecht. 1997. ATP synthase: an electrochemical transducer with rotatory mechanics. *TIBS.* 22:420–423.

Koradi, R., M. Billeter, and K. Wüthrich. 1996. MOLMOL: a program for display and analysis of macromolecular structures. *J. Mol. Graph.* 14:51–55.

Lindahl, E., B. Hess, and D. van der Spoel. 2001. GROMACS 3.0: a package for molecular simulation and trajectory analysis. *J. Mol. Model.* 7:306–317.

Ma, J., T. C. Flynn, Q. Cui, A. G. W. Leslie, J. E. Walker, and M. Karplus. 2002. A dynamic analysis of the rotation mechanism for conformational change in F$_1$-ATPase. *Structure.* 10:921–931.

Masaike, T., N. Mitome, H. Noji, E. M. R. Yasuda, K. Kinosita, and M. Yoshida. 2000. Rotation of F$_1$-ATPase and the hinge residues of the β-subunit. *J. Exp. Biol.* 203:1–8.

Masaike, T., E. Muneyuki, H. Noji, K. Kinosita, and M. Yoshida. 2002. F$_1$-ATPase changes its conformation upon phosphate release. *J. Biol. Chem.* 277:21643–21649.

Menz, R. I., J. E. Walker, and A. G. W. Leslie. 2001. Structure of bovine mitochondrial F$_1$-ATPase with nucleotide bound to all three catalytic sites: implications for the mechanism of rotary catalysis. *Cell.* 106:331–341.

Merritt, E. A., and D. J. Bacon. 1997. RASTER 3D: photorealistic molecular graphics. *Methods Enzymol.* 277:505–524.

Miwa, K., and M. Yoshida. 1989. The $\alpha_3\beta_3$ complex, the catalytic core of F$_1$-ATPase. *Proc. Natl. Acad. Sci. USA.* 86:6484–6487.

Miyamoto, S., and P. A. Kollman. 1992. SETTLE—an analytical version of the SHAKE and RATTLE algorithm for rigid water models. *J. Comp. Chem.* 13:952–962.

Noji, H., R. Yasuda, M. Yoshida, and K. Kinosita. 1997. Direct observation of the rotation of F$_1$-ATPase. *Nature.* 386:299–302.

Orriss, G., A. Leslie, K. Braig, and J. Walker. 1998. Bovine F$_1$-ATPase covalently inhibited with 4-chloro-7-nitrobenzofurazan: the structure provides further support for a rotary catalytic mechanism. *Structure.* 6:831–837.

Oster, G., and H. Y. Wang. 2000. Why is the mechanical efficiency of F$_1$-ATPase so high? *J. Bioenerg. Biomem.* 32:459–469.

Pänke, O., K. Gumbiowski, W. Junge, and S. Engelbrecht. 2000. F-ATPase: specific observation of the rotating c subunit oligomer of EF$_o$EF$_1$. *FEBS Lett.* 472:34–38.

Sabbert, D., S. Engelbrecht, and W. Junge. 1996. Intersubunit rotation in active F-ATPase. *Nature.* 381:623–625.

Sambongi, Y., Y. Iko, M. Tanabe, H. Omote, A. I.-K. I. Ueda, T. Yanagida, Y. Wada, and M. Futai. 1999. Mechanical rotation of the c subunit oligomer in ATP synthase (F$_o$F$_1$): direct observation. *Science.* 286:1722–1724.

Seelert, H., A. Poetsch, N. A. Dencher, A. Engel, H. Stahlberg, and D. J. Müller. 2000. Structural biology—proton-powered turbine of a plant motor. *Nature.* 405:418–419.

Shirakihara, Y., A. G. W. Leslie, J. P. Abrahams, J. E. Walker, T. Ueda, Y. Sekimoto, M. Kambara, K. Saika, Y. Kagawa, and M. Yoshida. 1997. The crystal structure of the nucleotide-free $\alpha_3\beta_3$ subcomplex of F$_1$-ATPase from the thermophilic *Bacillus PS3* is a symmetric trimer. *Structure.* 5:825–836.

Stahlberg, H., D. J. Müller, K. Suda, D. Fotiadis, A. Engel, T. Meier, U. Matthey, and P. Dimroth. 2001. Bacterial Na$^+$-ATP synthase has an undecameric rotor. *EMBO Rep.* 2:229–233.

Stock, D., A. G. W. Leslie, and J. E. Walker. 1999. Molecular architecture of the rotary motor in ATP synthase. *Science.* 286:1700–1705.

van Raaij, M., J. P. Abrahams, A. G. W. Leslie, and J. E. Walker. 1996. The structure of bovine F$_1$-ATPase complexed with the antibiotic inhibitor aurovertin B. *Proc. Natl. Acad. Sci. USA.* 93:6913–6917.

Wang, H., and G. Oster. 1998. Energy transduction in the F$_1$ motor of ATP synthase. *Nature.* 396:279–282.

Weber, J., S. Wilke-Mounts, R. S. F. Lee, E. Grell, and A. E. Senior. 1993. Specific placement of tryptophan in the catalytic sites of *Escherichia coli* F$_1$-ATPase provides a direct probe of nucleotide-binding—maximal ATP hydrolysis occurs with three sites occupied. *J. Biol. Chem.* 268:20126–20133.

Yasuda, R., H. Noji, K. Kinosita, and M. Yoshida. 1998. F$_1$-ATPase is a highly efficient molecular motor that rotates with discrete 120° steps. *Cell.* 93:1117–1124.

Yasuda, R., H. Noji, M. Yoshida, K. Kinosita, and H. Itoh. 2001. Resolution of distinct rotational substeps by submillisecond kinetic analysis of F$_1$-ATPase. *Nature.* 410:898–904.

Zhou, Y. T., T. M. Duncan, and R. L. Cross. 1997. Subunit rotation in *Escherichia coli* F$_o$F$_1$-ATP synthase during oxidative phosphorylation. *Proc. Natl. Acad. Sci. USA.* 94:10583–10587.